



HAL
open science

Low Temperature Rate Constants for the Reactions of O(1 D) with N₂, O₂, and Ar

Romain Grondin, Jean-Christophe J.-C. Loison, Kevin Hickson

► **To cite this version:**

Romain Grondin, Jean-Christophe J.-C. Loison, Kevin Hickson. Low Temperature Rate Constants for the Reactions of O(1 D) with N₂, O₂, and Ar. *Journal of Physical Chemistry A*, 2016, 120 (27), pp.4838-4844. 10.1021/acs.jpca.5b12358 . hal-03104578

HAL Id: hal-03104578

<https://hal.science/hal-03104578>

Submitted on 13 Jan 2021

HAL is a multi-disciplinary open access archive for the deposit and dissemination of scientific research documents, whether they are published or not. The documents may come from teaching and research institutions in France or abroad, or from public or private research centers.

L'archive ouverte pluridisciplinaire **HAL**, est destinée au dépôt et à la diffusion de documents scientifiques de niveau recherche, publiés ou non, émanant des établissements d'enseignement et de recherche français ou étrangers, des laboratoires publics ou privés.

Low Temperature Rate Constants for the Reactions of O(¹D) with N₂, O₂ and Ar

Romain Grondin,^{1,2} Jean-Christophe Loison^{1,2} and Kevin M. Hickson^{1,2}*

¹Université de Bordeaux, Institut des Sciences Moléculaires, UMR 5255, F-33400 Talence,
France

²CNRS, Institut des Sciences Moléculaires, UMR 5255, F-33400 Talence, France

Abstract

The kinetics of the gas-phase quenching reactions O(¹D) + N₂, O(¹D) + O₂ and O(¹D) + Ar have been studied over the 50 - 296 K temperature range using the Laval nozzle method. O(¹D) atoms were created in-situ by the pulsed photolysis of O₃ precursor molecules at 266 nm. Rate constants for these processes were measured directly, following the decay of O(¹D) atoms through vacuum ultra violet laser induced fluorescence at 115.215 nm. For the O(¹D) + N₂ and O(¹D) + O₂ reactions, the quenching efficiencies are seen to increase as the temperature falls. For the O(¹D) + N₂ system, this indicates the likely influence of the intermediate complex lifetime on the quenching rate through non-adiabatic processes. For the O(¹D) + O₂ system which is considerably more complex, this behavior could result from the interactions between several potential energy surfaces.

1 Introduction

Measurements of the rate constants for both reactive and non reactive collision processes involving electronically excited oxygen atoms, O(¹D), are widespread over the 200 – 300 K temperature range^{1, 2, 3, 4, 5, 6, 7} due to the importance of such processes in the chemistry of the Earth's atmosphere. In the stratosphere and troposphere particularly, the ultraviolet photodissociation of ozone, O₃, leads to the production of both ground state atomic oxygen O(³P) and O(¹D) with varying quantum yields depending on the wavelength of the incident light. The steady state concentration of O(¹D) atoms is generally low, due to their high reactivity with many important trace species such as H₂, CH₄, H₂O and N₂O, which act as major sources of the hydroxyl radical, OH, and nitric oxide, NO in both the troposphere and the stratosphere. O(¹D) is also lost by quenching through collisions with the major atmospheric constituents N₂ and O₂ to yield O(³P) atoms.



The fate of O(¹D) depends crucially on the competition between reactive losses and quenching. Chemical models of the Earth's atmosphere thus require data in the form of temperature dependent rate constants for these processes to correctly simulate the mole fractions of a wide range of molecules, given the lower reactivity of O(³P) towards atmospheric trace molecules and the particular importance of the OH radical as an atmospheric oxidant.

Previous experimental studies of O(¹D) reactions have been facilitated by the presence of readily available photolytic sources of these atoms (such as N₂O and O₃) while several different methods have been employed to follow the kinetics. The majority of previous studies have employed indirect detection methods. For investigations where quenching was the primary channel, O(¹D) loss can be determined from the temporal evolution of product O(³P)

formation, following $O(^3P)$ by resonance absorption⁸ or resonance fluorescence around 130 nm.^{1,2} In a similar manner for reactive processes, $O(^1D)$ reactivity can be determined by following the formation kinetics of molecular products such as OH radicals.⁹ An indirect method which has been shown to be particularly sensitive employs the $O(^1D) + C_2H$ reaction to trace $O(^1D)$ kinetics through the detection of chemiluminescent emission from $CH(A^2\Delta)$ radicals.^{3,4,10} In terms of direct detection methods, $O(^1D)$ can be followed by emission spectroscopy through the spin-forbidden $O(^1D) \rightarrow O(^3P)$ transition at 630 nm although this process has a low transition probability. As a result, elevated $O(^1D)$ concentrations are typically employed, potentially increasing the risk of secondary reactions.^{6,7} Earlier resonance absorption studies^{11,12} and more recent vacuum ultraviolet laser induced fluorescence measurements (VUV LIF)^{9,13,14} have employed the $3s\ ^1D - 2p\ ^1D$ transition at 115.2 nm to investigate the kinetics of $O(^1D)$ deactivation. Absorption measurements of this type also require the use of elevated $O(^1D)$ concentrations due to issues with sensitivity, while the VUV LIF experiments are likely to be the most accurate given the lower potential for secondary reactions corresponding with the use of lower radical concentrations.

Both reactions (1) and (2) have been studied on numerous occasions at room temperature, leading to recommended¹⁵ room temperature rate constant values of $(3.1 \pm 0.3) \times 10^{-11} \text{ cm}^3 \text{ molecule}^{-1} \text{ s}^{-1}$ and $(3.95 \pm 0.40) \times 10^{-11} \text{ cm}^3 \text{ molecule}^{-1} \text{ s}^{-1}$ respectively, based on the studies of Ravishankara et al.¹⁶ for reaction (1) and Blitz et al.,⁹ Amimoto et al.,¹¹ Lee and Slinger,¹⁷ Davidson et al.,⁷ Dunlea and Ravishankara,¹ Streit et al.,⁶ Strekowski et al.² and Takahashi et al.¹⁴ for reaction (2). The recommended temperature dependence for reaction (1) is taken from Ravishankara et al.¹⁶ as before, whereas the recommended temperature dependence for reaction (2) was calculated by normalizing the results of Strekowski et al.,² Dunlea and Ravishankara¹ and Streit et al.⁶ to the recommended room temperature value given above.

Streit et al.⁶ in particular measured the rates of both reactions (1) and (2) over an extended temperature range, from 354 K down to 104 K, demonstrating that both of these processes present slight negative temperature dependences. Such observations are highly indicative of the role played by complex formation in the quenching process. As bimolecular product formation is thermodynamically unfavourable in both of these cases, and stabilization of the association complexes (N_2O and O_3) can only occur at high pressure, reaction occurs primarily through non-adiabatic transitions. In the case of reaction (1), the spin-forbidden quenching process could arise due to spin-orbit couplings between the ground $X^1\Sigma^+$ state and the excited $^3A'$ and $^3A''$ states of N_2O leading to $\text{O}(^3\text{P})$ and $\text{N}_2(X^1\Sigma_g^+)$ as products. In the case of reaction (2), the $\text{O}(^1\text{D}) + \text{O}_2(X^3\Sigma_g^-)$ system is close in energy to the potential products $\text{O}(^3\text{P}) + \text{O}_2(b^1\Sigma_g^+)$ and/or $\text{O}(^3\text{P}) + \text{O}_2(a^1\Delta_g)$. As a result, no change of spin is required although a non-adiabatic transition $A' \rightarrow A''$ or $A'' \rightarrow A'$ is thought to be necessary for quenching to occur.¹⁸

In this paper, we report measurements of reactions (1) and (2) and of the $\text{O}(^1\text{D}) + \text{Ar}$ quenching reaction, at temperatures beyond those previously obtained, extending the kinetic data for these systems down to 50 K. A supersonic flow reactor coupled with direct VUV LIF detection of $\text{O}(^1\text{D})$ atoms at 115.2 nm is employed in the present work. The methodology used in this investigation is described in section 2. Section 3 presents the experimental results and discusses these values within the context of earlier work. Finally, our conclusions are presented in section 4.

2 Experimental Methodology

The experimental work in this paper employed a continuous flow supersonic reactor previously described,¹⁹ with other relevant details for the present study given in later work.^{20,21} Three different Laval nozzles were used to perform these experiments at specific temperatures of 127 K, 75 K and 50 K, with room temperature experiments (296 K) being

conducted without a Laval nozzle at reduced flow velocities. It was only possible to use argon based nozzles for this investigation as quenching of $O(^1D)$ is too efficient for N_2 to be used as the carrier gas. The calculated and measured flow properties obtained from independent calibration experiments are listed in Table 1.

Table 1 Continuous supersonic flow characteristics

Laval nozzle	Mach2 Ar	Mach3 Ar	Mach4 Ar
Mach number	2.0 ± 0.03^a	3.0 ± 0.1	3.9 ± 0.1
Carrier gas	Ar	Ar	Ar
Density ($\times 10^{16} \text{ cm}^{-3}$)	12.6	14.7	25.9
Impact pressure (Torr)	10.5	15.3	29.6
Stagnation pressure (Torr)	13.9	34.9	113
Temperature (K)	127 ± 2^a	75 ± 2	50 ± 1
Mean flow velocity (ms^{-1})	419 ± 3^a	479 ± 3	505 ± 1

^aThe errors on the Mach number, temperature and mean flow velocity, cited at the level of one standard deviation from the mean are calculated from separate measurements of the impact pressure using a Pitot tube as a function of distance from the Laval nozzle and the stagnation pressure within the reservoir.

O_3 was used as the source of $O(^1D)$ atoms in these experiments. To create O_3 , a small flow of O_2 was passed into an absorption cell held at approximately 700 Torr, which was irradiated by the continuous output of a high pressure mercury lamp through UV grade quartz windows. The UV photolysis of O_2 , followed by the three body recombination of $O(^3P)$ atoms with O_2 resulted in the formation of low concentrations of O_3 within the cell. The output of the cell was connected to the Laval nozzle reservoir where it was mixed with the main carrier gas flows and the coreagent O_2 or N_2 molecules. $O(^1D)$ atoms were produced in-situ by the 10 Hz photodissociation of O_3 at 266 nm with pulse energies around 21 mJ. The photolysis laser beam was aligned along the supersonic flow axis. Previous work¹⁵ has shown that the

quantum yield for O(¹D) formation at this wavelength is approximately 0.9 with the remaining part leading to O(³P) formation. The association reaction of O(³P) with O₂ to reform O₃ is not expected to be efficient under our low pressure experimental conditions, even at the lowest temperatures. O(¹D) atoms were detected directly on resonance through VUV LIF using the 3s ¹D – 2p ¹D transition at 115.215 nm. Light at and around this wavelength was generated by frequency doubling the output of a narrow band tuneable dye laser operating at 691.29 nm in a beta barium borate crystal, before focusing the resulting 345.645 nm light into a cell containing 100 Torr of Xenon with 230 Torr of Argon added for phase matching. The VUV light produced by frequency tripling in Xenon was collimated by a magnesium fluoride (MgF₂) lens at the exit of the cell. The tripling cell itself was placed at the level of the observation axis, perpendicular to the supersonic flow. The fluorescence from O(¹D) atoms within the supersonic flow was collected using a solar blind photomultiplier tube (PMT) which was isolated from the flow reactor by an MgF₂ window. The zone between the PMT and the window was maintained under vacuum to prevent supplementary losses of the VUV light by atmospheric absorption. A second MgF₂ lens within the evacuated volume was used to focus the O(¹D) fluorescence emission onto the PMT photocathode. The PMT output was fed into a boxcar integrator coupled to a PC for signal acquisition. O(¹D) VUV LIF signals were recorded as a function of time between the photolysis and probe lasers with the timing being controlled by a delay generator. 30 laser shots were averaged at each time point, with each kinetic decay consisting of at least 40 intervals. To establish the baseline signal, several time points were recorded at negative time delays, that is, with the probe laser firing before the photolysis laser.

The gases used in the experiments (Ar 99.999%, N₂ 99.999%, O₂ 99.999%, Xe 99.998%) were flowed from cylinders without purification into calibrated mass flow controllers,

allowing us to calculate the reagent, precursor and carrier gas concentrations from the ratios of the flow and the calculated flow density.

3 Results and Discussion

Exemplary decays of the O(¹D) fluorescence signal obtained at 50 K in the presence of excess N₂ and the carrier gas Ar, and in the presence of Ar alone are shown in Figure 1.

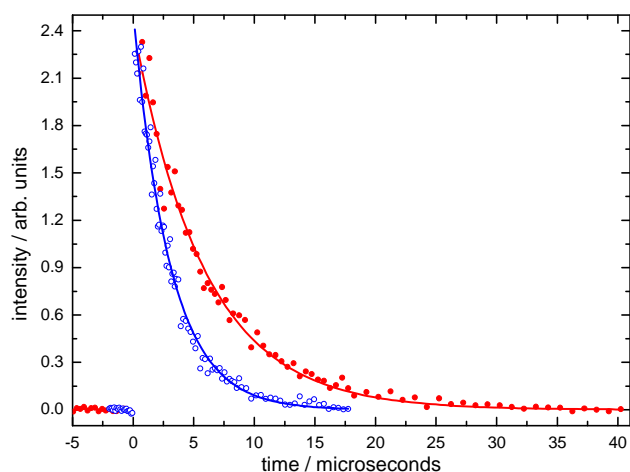


Figure 1 O(¹D) VUV LIF intensity as a function of time recorded at 50 K. (Red solid circles) O(¹D) quenching in the presence of the carrier gas Ar alone ($[\text{Ar}] = 2.59 \times 10^{17} \text{ molecule cm}^{-3}$); (Blue open circles) O(¹D) quenching in the presence of the carrier gas Ar ($[\text{Ar}] = 2.59 \times 10^{17} \text{ molecule cm}^{-3}$) with added N₂ ($[\text{N}_2] = 2.56 \times 10^{15} \text{ molecule cm}^{-3}$).

Simple exponential fits to traces such as those presented in Figure 1 allowed us to determine pseudo-first-order rate constants for O(¹D) loss from the time constant of the decay profile. In such experiments, taking the measurements of reaction (1) as an example, several processes potentially lead to O(¹D) loss, including:





O_2 is present in the flow at all times at low concentrations ranging from $(5 - 7) \times 10^{13}$ molecule cm^{-3} , even for our measurements of reaction (1) due to its use as a precursor for O_3 formation, although this represents a small constant contribution to the overall loss rate ($[\text{O}_2]_{\text{precursor}}$ is fixed for any series of measurements). It can be seen from Figure 1 that $\text{O}(^1\text{D})$ is more efficiently removed when N_2 is added to the cold supersonic flow, although collisions of $\text{O}(^1\text{D})$ with Ar alone also lead to its rapid deactivation through reaction (3). Nevertheless, $[\text{Ar}]$ is also fixed for any series of measurements. Earlier studies of reaction (3) over the range 110 - 330 K,^{22,23,24,25,26} have determined the rate constant for this process to be around 5×10^{13} cm^3 molecule⁻¹ s⁻¹ with little variation as a function of temperature. In the examples presented above, the pseudo-first-order rates for $\text{O}(^1\text{D})$ loss are calculated to be 1.62×10^5 s⁻¹ with Ar alone and 3.40×10^5 s⁻¹ with added N_2 . $\text{O}(^1\text{D})$ could also be lost through reaction (4). In this case, it is difficult to make an accurate determination of the O_3 concentration within the supersonic flow itself. However, if we estimate that 5 % at most of the initial O_2 is converted to O_3 (which is likely to be a significant overestimate of the O_3 production efficiency), $[\text{O}_3]$ will be in the range $(5 - 7) \times 10^{12}$ molecule cm^{-3} . As the rate constant for reaction (4) has been measured to have a weakly temperature dependent value around 2.5×10^{-10} cm^3 molecule⁻¹ s⁻¹,¹⁵ this reaction will contribute at most 1750 s⁻¹ to the decay; a negligible quantity given the range of the overall pseudo-first-order rate constants measured here. $\text{O}(^1\text{D})$ will also be lost through diffusion as described by reaction (5). In these experiments, it is not possible to measure the diffusional loss rate of $\text{O}(^1\text{D})$ directly given the high deactivation rate with the carrier gas Ar in particular. Nevertheless, its value is likely to be comparable to diffusional loss rates obtained in our earlier experiments under similar conditions on atomic species of similar mass such as $\text{C}(^3\text{P})$.²⁰ In this case, diffusional loss of $\text{C}(^3\text{P})$ was found to be of the order of a few thousand s⁻¹ for all Laval nozzles used. As a

result, this process represents a very minor contribution to the total pseudo-first-order decay rate of $O(^1D)$ in these experiments.

To determine the second-order rate constants at a given temperature, several different coreagent N_2 and O_2 concentrations were used and the pseudo-first-order rate constants were plotted against the corresponding coreagent concentration as shown in Figure 2.

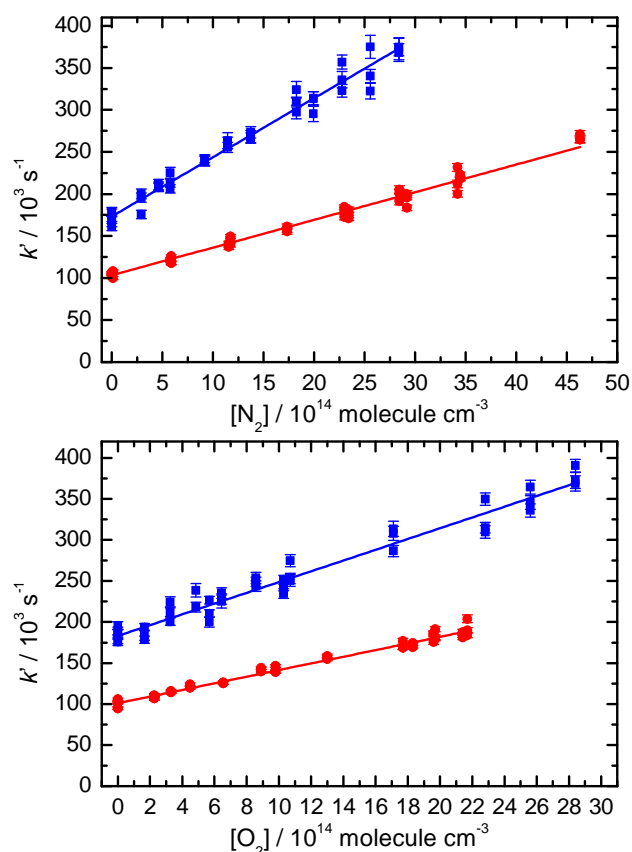


Figure 2 Second-order plots for the $O(^1D) + N_2$ (upper panel) and $O(^1D) + O_2$ (lower panel) reactions. (Blue solid circles) pseudo-first order rate constants as a function of excess coreagent concentration recorded at 50 K. (Red solid circles) pseudo-first order rate constants as a function of excess coreagent concentration recorded at 296 K. The pseudo-first order rates and their associated statistical uncertainties are determined from fits to decay profiles such as those displayed in Figure 1. The solid lines represent weighted linear least squares fits to the data to yield the second-order rate constant from the slope.

The value of the slope of all of these plots (weighted by the calculated uncertainties of fits to the individual decay profiles) equates to the rate constant at a specified temperature. The y-axis intercept value of all of these plots is seen to be large, corresponding to the loss of O(¹D) atoms mostly through collisions with the carrier gas Ar. In this respect, it was also possible to determine second-order rate constants for reaction (3) from kinetic decays recorded in the absence of coreagent O₂ or N₂, similar to the one shown in Figure 1. As discussed above, the y-axis intercept value k' at any given temperature is composed of several contributions:

$$k' = k_{\text{O}(1\text{D}+\text{Ar})}[\text{Ar}] + k_{\text{O}(1\text{D}+\text{O}_2\text{precursor})}[\text{O}_2]_{\text{precursor}} + k_{\text{O}(1\text{D}+\text{O}_3)}[\text{O}_3] + k_{\text{diff}}$$

where the terms $k_{\text{O}(1\text{D}+\text{O}_3)}[\text{O}_3]$ and k_{diff} are considered to be negligibly small in the present experiments. The contribution from the term $k_{\text{O}(1\text{D}+\text{O}_2\text{precursor})}[\text{O}_2]_{\text{precursor}}$ can be evaluated from the product of the O₂ precursor concentration and the rate constant of reaction (2) determined here from the slope of the second order plot with coreagent O₂ at the appropriate temperature (see Figure 2). Although this is not the usual method employed to extract second-order reaction rates (see description above and Figure 2), the total gas density is fixed for any specific nozzle so that it was impossible to vary this quantity at 50 K, 75 K and 127 K. Nevertheless, at least 22 values of k' were recorded at a fixed [Ar] at each of these temperatures to reduce potential errors from scatter in the experimental data. The mean temperature dependent rate constants determined in this way are summarized in Table 2 and are plotted in Figure 3 alongside the previous experimental work. As an additional verification that this method yielded the same result as the one obtained from the slope of second-order plots, we also conducted experiments at 296 K where pseudo first order rate constants for reaction (3) were recorded over a range of Ar concentrations by varying the total pressure. The rate constant of $(5.6 \pm 0.6) \times 10^{-13} \text{ cm}^3 \text{ molecule}^{-1} \text{ s}^{-1}$ measured by this method is in good agreement with the value determined at a fixed [Ar]. Rate constants for the O(¹D) +

N_2 and $\text{O}(^1\text{D}) + \text{O}_2$ reactions are presented as a function of temperature in Figures 4 and 5 respectively.

Table 2 Temperature dependent rate constants for the $\text{O}(^1\text{D}) + \text{Ar}$ reaction

T / K	$[\text{Ar}] / 10^{17} \text{ cm}^{-3}$	N^b	$k_{\text{O}(^1\text{D})+\text{Ar}} / \text{cm}^3 \text{ s}^{-1}$
296	1.6	22	$(6.1 \pm 0.6)^c \times 10^{-13}$
296	0.8 - 3.2	8	$(5.6 \pm 0.6) \times 10^{-13}$
127 ± 2^a	1.26	24	$(5.8 \pm 0.6) \times 10^{-13}$
75 ± 2	1.5	24	$(6.8 \pm 0.7) \times 10^{-13}$
50 ± 1	2.6	23	$(6.8 \pm 0.7) \times 10^{-13}$

^aUncertainties on the calculated temperatures represent the statistical (1σ) errors obtained from Pitot tube measurements of the impact pressure. ^bNumber of individual measurements. ^cUncertainties on the measured rate constants represent the combined statistical (1σ) and estimated systematic (10%) errors.

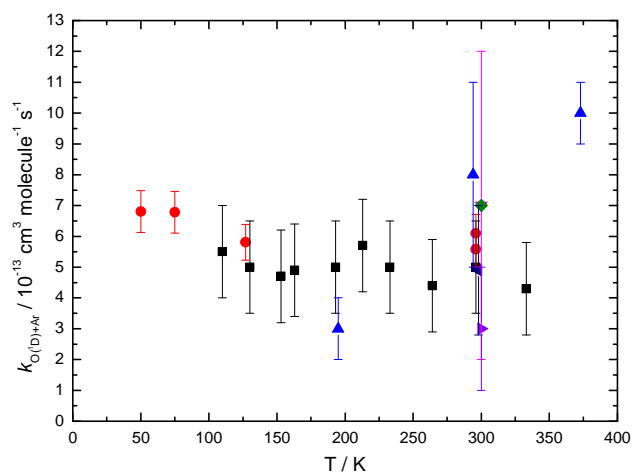


Figure 3 Rate constants for the $\text{O}(^1\text{D}) + \text{Ar}$ reaction as a function of temperature. (Red filled circles) This work; (Black filled squares) Davidson et al.;²² (Blue filled triangles) Blitz et al.;⁹ (Pink filled triangle) Preston & Cvetanovic;²³ (Green filled diamond) Heidner & Husain;²⁴

(Blue open diamond) Klemm & Stief;²⁵ (Purple triangle) Schofield.²⁶ The Blitz et al. value at 673 K is omitted for clarity.

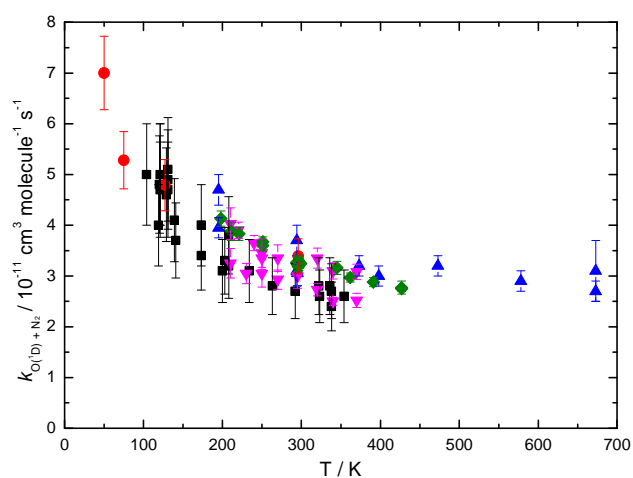


Figure 4 Rate constants for the $O(^1D) + N_2$ reaction as a function of temperature. (Red filled circles) This work; (Black filled squares) Streit et al.,⁶ (Blue filled triangles) Blitz et al.,⁹ (Pink filled triangles) Dunlea & Ravishankara,¹ (Green filled diamonds) Strekowski et al.²

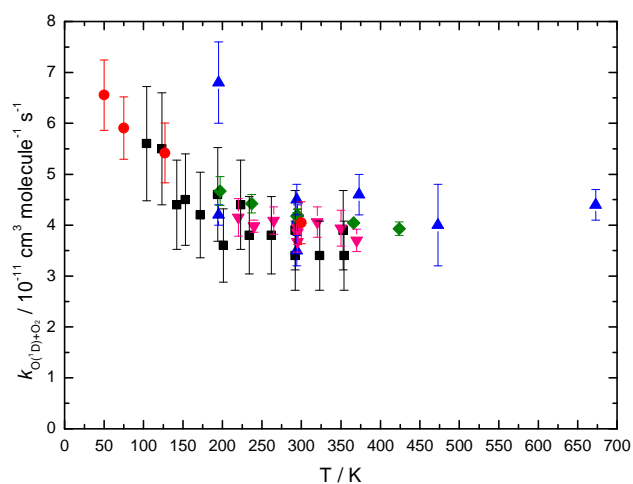


Figure 5 Rate constants for the $O(^1D) + O_2$ reaction as a function of temperature. (Red filled circles) This work; (Black filled squares) Streit et al.,⁶ (Blue filled triangles) Blitz et al.,⁹ (Pink filled triangles) Dunlea & Ravishankara,¹ (Green filled diamonds) Strekowski et al.²

Table 3 Temperature dependent rate constants for the $O(^1D) + N_2$ and $O(^1D) + O_2$ reactions

T / K	N^b	$[\text{N}_2]/10^{14} \text{ cm}^{-3}$	$k_{\text{O}(1\text{D})+\text{N}_2} / \text{cm}^3 \text{ s}^{-1}$	N^b	$[\text{O}_2]/10^{14} \text{ cm}^{-3}$	$k_{\text{O}(1\text{D})+\text{O}_2} / \text{cm}^3 \text{ s}^{-1}$
296	42	0-46	$(3.4 \pm 0.3)^c \times 10^{-11}$	48	0-22	$(4.0 \pm 0.4)^c \times 10^{-11}$
127 ± 2^a	42	0-20	$(4.8 \pm 0.5) \times 10^{-11}$	36	0-9	$(5.4 \pm 0.6) \times 10^{-11}$
75 ± 2	42	0-17	$(5.3 \pm 0.6) \times 10^{-11}$	42	0-17	$(5.9 \pm 0.6) \times 10^{-11}$
50 ± 1	38	0-28	$(7.0 \pm 0.7) \times 10^{-11}$	41	0-28	$(6.6 \pm 0.7) \times 10^{-11}$

^aUncertainties on the calculated temperatures represent the statistical (1σ) errors obtained from Pitot tube measurements of the impact pressure. ^bNumber of individual measurements. ^cUncertainties on the measured rate constants represent the combined statistical (1σ) and estimated systematic (10%) errors.

It can be seen from Figure 3 that the rate constants for reaction (3) measured here are generally in good agreement with earlier work at both room temperature^{23,24,25,26} and below,²² with the exception of the data of Blitz et al.⁹ In common with the previous work by Davidson et al.,²² we find very little variation of the rate constant for the $\text{O}(^1\text{D}) + \text{Ar}$ reaction over the 50 - 296 K range although the slight increase observed as the temperature falls would seem to be a real effect. In this system, a bound ArO intermediate is formed in its $^1\Sigma^+$ state, correlating with the $\text{O}(^1\text{D}) + \text{Ar}(^1\text{S}_0)$ reagents. The $^1\Sigma^+$ state crosses two repulsive triplet states ($^3\Pi$ or $^3\Sigma^-$) which correlate with ground state products $\text{O}(^3\text{P}) + \text{Ar}(^1\text{S}_0)$. Reaction occurs via a non-adiabatic transition from the $^1\Sigma^+$ state to one or both of the triplet states through spin-orbit coupling. Given the weak temperature dependence of the rate constant, the present results show that reaction (3) occurs in the absence of an activation barrier, confirming that that crossing point for the $^1\Sigma^+$ potential energy surface (PES) and the triplet PESs occurs on the long range attractive part of the singlet PES, below the $\text{O}(^1\text{D}) + \text{Ar}$ asymptote. The slightly faster rate at lower temperature may be the result of various effects such as the long-range interactions. From a semi-classical point of view there are only two passages at the singlet-triplet crossing point so that the temperature should have little influence on the singlet to

triplet crossing efficiency of the O(¹D) + Ar system. It may slightly increase with decreasing temperature as the nuclear velocity at the crossing point decreases, leading to a slightly more efficient crossing according to the Landau-Zener formalism.

The non-adiabatic quenching dynamics of reaction (1) were recently investigated in detail by Defazio et al. using a coupled channel real wave packet approach employing the ¹A', ³A' and ³A'' PESs of N₂O.²⁷ They found that spin-orbit coupling between the ¹A' surface correlating with O(¹D) + N₂ reagents and the ³A'' surface correlating with O(³P) + N₂ products was the main pathway for quenching, over and above the ¹A' → ³A' one. These authors calculated rate constants at 300 K for quenching from O(¹D) + N₂ (*j* = 0) and O(¹D) + N₂ (*j* = 1) of $1.3 \times 10^{-11} \text{ cm}^3 \text{ molecule}^{-1} \text{ s}^{-1}$ and $1.5 \times 10^{-11} \text{ cm}^3 \text{ molecule}^{-1} \text{ s}^{-1}$ respectively. Although it is not possible to compare directly with the experimentally determined rates, as at least 16 rotational levels of N₂ are significantly populated at room temperature, these values are nonetheless reasonably close to the recommended room temperature rate¹⁵ of $3.1 \times 10^{-11} \text{ cm}^3 \text{ molecule}^{-1} \text{ s}^{-1}$. It can be seen from Figure 4 that the value of the rate constant for reaction (1) of $(3.4 \pm 0.3) \times 10^{-11} \text{ cm}^3 \text{ molecule}^{-1} \text{ s}^{-1}$ determined in the present study at 296 K is in good agreement with this evaluation. In terms of the temperature dependence of the quenching rate, previous work has shown that the rate constant for this process displays a negative temperature dependence, becoming faster as the temperature falls. Indeed, earlier measurements by Streit et al.⁶ over an extended temperature range measured rate constants that increase by approximately 60 % to a value around $5.0 \times 10^{-11} \text{ cm}^3 \text{ molecule}^{-1} \text{ s}^{-1}$ at 104 K, with a noticeable enhancement of the effect at the lowest temperatures. The present investigation confirms this trend with a measured value of the rate constant for reaction (1) at 127 K of $(4.8 \pm 0.5) \times 10^{-11} \text{ cm}^3 \text{ molecule}^{-1} \text{ s}^{-1}$. At even lower temperatures, the O(¹D) + N₂ quenching rate is seen to accelerate, reaching a value of $(7.0 \pm 0.7) \times 10^{-11} \text{ cm}^3 \text{ molecule}^{-1} \text{ s}^{-1}$

at 50 K, more than double the recommended room temperature rate. Such an increase is clearly an indication of the role played by the lifetime of the bound $^1\Sigma^+$ state of N_2O in the quenching process as highlighted by Defazio et al.²⁷ Indeed, previous work^{27,28,29} has confirmed that at low collision energies, long-lived resonances associated with the formation of metastable complexes exist which could enhance the probability for spin orbit coupling to occur. A fit of the form $k(T) = A \exp(B/T)$ to the combined datasets shown in Figure 4 yields the parameters $A = (2.53 \pm 0.05) \times 10^{-11} \text{ cm}^3 \text{ molecule}^{-1} \text{ s}^{-1}$ and $B = 69 \pm 6$.

The mechanism of the $\text{O}(^1\text{D}) + \text{O}_2$ reaction is complex, giving rise to the formation of ground state $\text{O}(^3\text{P})$ atoms and electronically excited O_2 in either the $\text{b}^1\Sigma_g^+$ state or the $\text{a}^1\Delta_g$ state. Several early papers,^{30,31} conclusively showed that $\text{O}_2(\text{b}^1\Sigma_g^+)$ is preferentially formed. Indeed, emission from the magnetic dipole allowed $\text{O}_2(\text{b}^1\Sigma_g^+) \rightarrow \text{O}_2(\text{X}^3\Sigma_g^-)$ transition (the so called “oxygen atmospheric bands”) is readily observed and can even be used to follow the progress of reaction (2). It can be seen from Figure 5 that the measured room temperature rate constant for the $\text{O}(^1\text{D}) + \text{O}_2$ reaction of $(4.0 \pm 0.4) \times 10^{-11} \text{ cm}^3 \text{ molecule}^{-1} \text{ s}^{-1}$ is in excellent agreement with the currently recommended value of $3.95 \times 10^{-11} \text{ cm}^3 \text{ molecule}^{-1} \text{ s}^{-1}$. In a similar manner to the rate constants for the $\text{O}(^1\text{D}) + \text{N}_2$ reaction, the rate is seen to increase as the temperature falls. In particular, Streit et al.⁶ measured rate constants for reaction (2) varying between $(3.4 - 5.6) \times 10^{-11} \text{ cm}^3 \text{ molecule}^{-1} \text{ s}^{-1}$ over the 354 K - 104 K range; in good agreement with our measurement of the rate constant at 127 K of $(5.4 \pm 0.6) \times 10^{-11} \text{ cm}^3 \text{ molecule}^{-1} \text{ s}^{-1}$. The value of the rate constant obtained by Blitz et al.⁹ at 195 K using the OH tracer method seems to be anomalously high when compared with the low temperature values obtained by other groups and is in disagreement with their own value determined by direct VUV LIF detection of $\text{O}(^1\text{D})$. The present study indicates that the quenching rate constant continues to increase below 100 K, reaching a value of $(6.6 \pm 0.7) \times 10^{-11} \text{ cm}^3 \text{ molecule}^{-1} \text{ s}^{-1}$ at 50 K, although the magnitude of the increase is less pronounced than for the $\text{O}(^1\text{D}) + \text{N}_2$ case.

A fit of the form $k(T) = A \exp(B/T)$ to the combined datasets shown in Figure 5 yields the parameters $A = (3.70 \pm 0.06) \times 10^{-11} \text{ cm}^3 \text{ molecule}^{-1} \text{ s}^{-1}$ and $B = 30 \pm 4$. The $\text{O}(^1\text{D}) + \text{O}_2(\text{X}^3\Sigma^-_g)$ reaction has been partially studied by Grebenshchikov et al.³² during their study of O_3 photodissociation at a high level of theory. However, due to the high density of triplet states of the $\text{O} + \text{O}_2$ reaction, the determination of the quenching pathways involves many states and it is a challenging problem to identify the specific states involved. Indeed, the $\text{O}(^1\text{D}) + \text{O}_2(\text{X}^3\Sigma^-)$ reaction involves the $7\text{A}'$ and $8\text{A}'$ states and the $7\text{A}''$, $8\text{A}''$ and $9\text{A}''$ triplet states of the global $\text{O} + \text{O}_2$ system. Grebenshchikov et al.³² calculated the $7\text{A}'$ and the $7\text{A}''$ states, showing that only the $7\text{A}''$ state presents purely non-repulsive behavior with a shallow van der Waals minimum followed by an avoided crossing with the $6\text{A}''$ state arising from $\text{O}(^3\text{P}) + \text{O}_2(^1\Sigma^+_g)$. The presence of the avoided crossing precludes the possibility of barrierless reaction through O_3 formation except through potentially non-adiabatic behavior such as through $\text{A}' \rightarrow \text{A}''$ or $\text{A}'' \rightarrow \text{A}'$ transitions.¹⁸ However there can be a direct reaction from $\text{O}(^1\text{D}) + \text{O}_2(\text{X}^3\Sigma^-_g)$ toward $\text{O}(^3\text{P}) + \text{O}_2(^1\Sigma^+_g)$ and/or $\text{O}(^3\text{P}) + \text{O}_2(^1\Delta_g)$ as both $\text{O}_2(^1\Sigma^+_g)$ and $\text{O}_2(^1\Delta_g)$ states are detected with high estimated branching ratios (McCullough & McGrath,³³ Donovan & Husain¹⁸). Precise calculations of the reaction mechanism to calculate the temperature dependence of the reaction rate and the product branching ratios of the individual channels would require a high level theoretical approach including the first eight A' and nine A'' states of the $\text{O} + \text{O}_2$ system.

4 Conclusions

An experimental investigation of the quenching reactions of $\text{O}(^1\text{D})$ with three different collision partners, O_2 , N_2 and Ar has been conducted over a range of temperatures using a continuous supersonic flow reactor, extending the available kinetic data for these processes to 50 K. $\text{O}(^1\text{D})$ was produced by pulsed laser photolysis of O_3 as the precursor molecule and the

excited atoms were followed directly through vacuum ultra violet laser induced fluorescence detection. The rate constants for all three processes are in excellent agreement with earlier experimental studies at higher temperatures. For the $O(^1D) + N_2$ and the $O(^1D) + O_2$ reactions, the quenching rate is seen to increase noticeably as the temperature falls, with the increase being more pronounced below 100 K. In the case of the $O(^1D) + N_2$ system, this effect can be explained by the formation of an energized N_2O complex intermediate whose lifetime increases at low temperature, enhancing the probability for non-adiabatic transitions through spin-orbit coupling. For the $O(^1D) + O_2$ system, an energized O_3 intermediate is also formed, although several potential pathways could be at the origin of the negative temperature dependence in this case. For the $O(^1D) + Ar$ reaction, despite the barrierless nature of the quenching pathway through a bound ArO intermediate, the low quenching rate constant values indicate that spin-orbit coupling is relatively inefficient for this system.

AUTHOR INFORMATION

Corresponding Author

* Correspondence to: km.hickson@ism.u-bordeaux1.fr. Tel: +33 (0)5 40 00 63 42

Author Contributions

The manuscript was written through contributions of all authors. All authors have given approval to the final version of the manuscript.

ACKNOWLEDGMENTS

JCL, KMH and RG acknowledge support from the INSU-CNRS national programs PCMI and PNP.

REFERENCES

1. Dunlea, E. J.; Ravishankara, A. R., Kinetic studies of the reactions of O(¹D) with several atmospheric molecules. *Phys. Chem. Chem. Phys.* **2004**, *6*, 2152.
2. Strekowski, R. S.; Nicovich, J. M.; Wine, P. H., Temperature-dependent kinetics study of the reactions of O(¹D₂) with N₂ and O₂. *Phys. Chem. Chem. Phys.* **2004**, *6*, 2145.
3. Vranckx, S.; Peeters, J.; Carl, S., A temperature dependence kinetic study of O(¹D) + CH₄: overall rate coefficient and product yields. *Phys. Chem. Chem. Phys.* **2008**, *10*, 5714-22.
4. Vranckx, S.; Peeters, J.; Carl, S., Kinetics of O(¹D) + H₂O and O(¹D) + H₂: absolute rate coefficients and O(³P) yields between 227 and 453 K. *Phys. Chem. Chem. Phys.* **2010**, *12*, 9213-21.
5. Dunlea, E. J.; Ravishankara, A. R., Measurement of the rate coefficient for the reaction of O(¹D) with H₂O and re-evaluation of the atmospheric OH production rate. *Phys. Chem. Chem. Phys.* **2004**, *6*, 3333-3340.
6. Streit, G. E.; Howard, C. J.; Schmeltekopf, A. L.; Davidson, J. A.; Schiff, H. I., Temperature-Dependence of O(¹D) Rate Constants for Reactions with O₂, N₂, CO₂, O₃, and H₂O. *J. Chem. Phys.* **1976**, *65*, 4761-4764.
7. Davidson, J. A.; Schiff, H. I.; Streit, G. E.; McAfee, J. R.; Schmeltekopf, A. L.; Howard, C. J., Temperature Dependence of O(¹D) Rate Constants for Reactions with N₂O, H₂, CH₄, HCl, and NH₃. *J. Chem. Phys.* **1977**, *67*, 5021.
8. Wine, P. H.; Ravishankara, A. R., kinetics of O(¹D) interactions with the atmospheric gases N₂, N₂O, H₂O, H₂, CO₂, and O₃. *Chem. Phys. Lett.* **1981**, *77*, 103-109.

9. Blitz, M. A.; Dillon, T. J.; Heard, D. E.; Pilling, M. J.; Trought, I. D., Laser induced fluorescence studies of the reactions of O(¹D₂) with N₂, O₂, N₂O, CH₄, H₂, CO₂, Ar, Kr and n-C₄H₁₀. *Phys. Chem. Chem. Phys.* **2004**, *6*, 2162.
10. Carl, S. A., A highly sensitive method for time-resolved detection of O(¹D) applied to precise determination of absolute O(¹D) reaction rate constants and O(³P) yields. *Phys. Chem. Chem. Phys.* **2005**, *7*, 4051-3.
11. Amimoto, S. T.; Force, A. P.; Gulotty, R. G.; Wiesenfeld, J. R., Collisional deactivation of O(2¹D₂) by the atmospheric gases. *J. Chem. Phys.* **1979**, *71*, 3640.
12. Heidner, R. F.; Husain, D., Quenching of O(2¹D₂) by atmospheric gases. *Nature-Physical Science* **1973**, *241*, 10-11.
13. Kono, M.; Matsumi, Y., Reaction processes of O(¹D) with fluoroethane compounds. *J. Phys. Chem. A* **2001**, *105*, 65-69.
14. Takahashi, K.; Takeuchi, Y.; Matsumi, Y., Rate constants of the O(¹D) reactions with N₂, O₂, N₂O, and H₂O at 295K. *Chem. Phys. Lett.* **2005**, *410*, 196-200.
15. Sander, S. P.; J. Abbatt; J. R. Barker; J. B. Burkholder; R. R. Friedl; D. M. Golden; R. E. Huie; C. E. Kolb; M. J. Kurylo; G. K. Moortgat; V. L. Orkin; Wine, P. H., Chemical Kinetics and Photochemical Data for Use in Atmospheric Studies, Evaluation No. 17. *JPL Publication 10-6, Jet Propulsion Laboratory, Pasadena, 2011* <http://jpldataeval.jpl.nasa.gov>. **2011**.
16. Ravishankara, A. R.; Dunlea, E. J.; Blitz, M. A.; Dillon, T. J.; Heard, D. E.; Pilling, M. J.; Strekowski, R. S.; Nicovich, J. M.; Wine, P. H., Redetermination of the rate coefficient for the reaction of O(¹D) with N₂. *Geophys. Res. Lett.* **2002**, *29*, 4.

17. Lee, L. C.; Slanger, T. G., Observations on $O(^1D \rightarrow ^3P)$ and $O_2(b^1\Sigma_g^+ \rightarrow X^3\Sigma_g^-)$ following O_2 photodissociation. *J. Chem. Phys.* **1978**, *69*, 4053.
18. Donovan, R. J.; Husain, D., Recent Advances in the Chemistry of Electronically Excited Atoms. *Chem. Rev.* **1970**, *70*, 489-516.
19. Daugey, N.; Caubet, P.; Bergeat, A.; Costes, M.; Hickson, K. M., Reaction kinetics to low temperatures. Dicarbon + acetylene, methylacetylene, allene and propene from $77 \leq T \leq 296$ K. *Phys. Chem. Chem. Phys.* **2008**, *10*, 729-737.
20. Shannon, R. J.; Cossou, C.; Loison, J.-C.; Caubet, P.; Balucani, N.; Seakins, P. W.; Wakelam, V.; Hickson, K. M., The fast $C(^3P) + CH_3OH$ reaction as an efficient loss process for gas-phase interstellar methanol. *RSC Adv.* **2014**, *4*, 26342.
21. Hickson, K. M.; Loison, J. C.; Guo, H.; Suleimanov, Y. V., Ring-Polymer Molecular Dynamics for the Prediction of Low-Temperature Rates: An Investigation of the $C(^1D) + H_2$ Reaction. *J. Phys. Chem. Lett.* **2015**, *6*, 4194-9.
22. Davidson, J. A.; Schiff, H. I.; Brown, T. J.; Streit, G. E.; Howard, C. J., Rate constants for the deactivation of $O(^1D)$ by Xe, Kr, and Ar over the range 110–330 K. *J. Chem. Phys.* **1978**, *69*, 1213.
23. Preston, K. F.; Cvetanovic, R. J., Collisional deactivation of excited oxygen atoms in photolysis of NO_2 at 2288 Å. *J. Chem. Phys.* **1966**, *45*, 2888-2893.
24. Heidner, R. F.; Husain, D., Study of Collisional Quenching Of $O(^2D_2)$ by Noble-Gases Employing Time-Resolved Attenuation of Atomic Resonance Radiation in Vacuum Ultraviolet. *Int. J. Chem. Kinet.* **1974**, *6*, 77-87.

25. Klemm, R. B.; Stief, L. J., Absolute Rate Parameters for Reaction of Ground-State Atomic Oxygen with Carbonyl Sulfide. *J. Chem. Phys.* **1974**, *61*, 4900-4906.
26. Schofield, K., Rate Constants for Gaseous Interactions of O(2^1D_2) and O(2^1S_0) - Critical Evaluation. *J. Photochem.* **1978**, *9*, 55-68.
27. Defazio, P.; Gamallo, P.; Petrongolo, C., Nonadiabatic dynamics of O(1D) + N $_2$ (X $^1\Sigma_g^+$) \rightarrow O(3P) + N $_2$ (X $^1\Sigma_g^+$) on three coupled potential surfaces: symmetry, Coriolis, spin-orbit, and Renner-Teller effects. *J. Chem. Phys.* **2012**, *136*, 054308.
28. Takayanagi, T., Quantum scattering calculations of the O(1D) + N $_2$ (X $^1\Sigma_g^+$) \rightarrow O(3P) + N $_2$ (X $^1\Sigma_g^+$) spin-forbidden electronic quenching collision. *J. Phys. Chem. A* **2002**, *106*, 4914-4921.
29. Chu, T. S.; Xie, T. X.; Han, K. L., Nonadiabatic energy transfer studies of O(1D) + N $_2$ (X $^1\Sigma_g^+$) \rightarrow O(3P) + N $_2$ (X $^1\Sigma_g^+$) by time-dependent wave packet. *J. Chem. Phys.* **2004**, *121*, 9352-9360.
30. Young, R. A.; Black, G.; Slanger, T. G., Reaction and Deactivation of O(1D). *J. Chem. Phys.* **1968**, *49*, 4758-4768.
31. Young, R. A.; Black, G., Deactivation of O(1D). *J. Chem. Phys.* **1967**, *47*, 2311-2318.
32. Grebenshchikov, S. Yu.; Qu, Z. W.; Zhu, H.; Schinke, R., New Theoretical Investigations of the Photodissociation of Ozone in the Hartley, Huggins, Chappuis, and Wulf bands. *Phys. Chem. Chem. Phys.* **2007**, *9*, 2044-2064.
33. McCullough, D. W.; McGrath, W. D., Electronic-Vibrational Energy Transfer in the Reaction of O(1D) Atoms with Molecular Oxygen. *J. Photochem.* **1972**, *1*, 241-253.